doi:10.1038/nature18645

Absence of 21st century warming on Antarctic Peninsula consistent with natural variability

John Turner[1], Hua Lu[1], Ian White[1], John C. King[1], Tony Phillips[1], J. Scott Hosking[1], Thomas J. Bracegirdle[1], Gareth J. Marshall[1], Robert Mulvaney[1] & Pranab Deb[1]

Since the 1950s, research stations on the Antarctic Peninsula have recorded some of the largest increases in near-surface air temperature in the Southern Hemisphere[1]. This warming has contributed to the regional retreat of glaciers[2], disintegration of floating ice shelves[3] and a 'greening' through the expansion in range of various flora[4]. Several interlinked processes have been suggested as contributing to the warming, including stratospheric ozone depletion[5], local sea-ice loss[6], an increase in westerly winds[5,7], and changes in the strength and location of low–high-latitude atmospheric teleconnections[8,9]. Here we use a stacked temperature record to show an absence of regional warming since the late 1990s. The annual mean temperature has decreased at a statistically significant rate, with the most rapid cooling during the Austral summer. Temperatures have decreased as a consequence of a greater frequency of cold, east-to-southeasterly winds, resulting from more cyclonic conditions in the northern Weddell Sea associated with a strengthening mid-latitude jet. These circulation changes have also increased the advection of sea ice towards the east coast of the peninsula, amplifying their effects. Our findings cover only 1% of the Antarctic continent and emphasize that decadal temperature changes in this region are not primarily associated with the drivers of global temperature change but, rather, reflect the extreme natural internal variability of the regional atmospheric circulation.

While global mean surface air temperature (SAT) has increased over recent decades, the rate of regional warming has varied markedly[10], with some of the most rapid SAT increases recorded in the polar regions[11–13]. In Antarctica, the largest SAT increases have been observed in the Antarctic Peninsula (AP) and especially on its west coast[1]: in particular, Vernadsky (formerly Faraday) station (Fig. 1) experienced an increase in annual mean SAT of 2.8 °C between 1951 and 2000.

The AP is a challenging area for the attribution of the causes of climate change because of the shortness of the *in situ* records, the large inter-annual circulation variability[14] and the sensitivity to local interactions between the atmosphere, ocean and ice. In addition, the atmospheric circulation of the AP and South Pacific are quite different between summer (December–February) and the remainder of the year.

Since the late 1970s, the springtime loss of stratospheric ozone has contributed to the warming of the AP, particularly during summer[7]. However, during the extended winter period of March–September, when teleconnections between the tropics and high southern latitudes are strongest[15], tropical sea surface temperature (SST) anomalies in the Pacific and Atlantic Oceans[16] can strongly modulate the climate of the AP. The teleconnections are further affected by the mid-latitude jet, which influences regional cyclonic activity and AP SATs. While the jet is strong for most of the year, during the summer it is weaker, there are fewer cyclones, and tropical forcing plays little part in AP climate variability.

The annual mean SAT records from six coastal stations located in the northern AP (Fig. 1) show a warming through the second half of the twentieth century, followed by little change or a decrease during the first part of the twenty-first century[17]. We investigate the differences in high and low latitude forcing on the climate of the AP during what we henceforth term the 'warming' and 'cooling' periods, focusing particularly on the period since 1979, since this marks the start of the availability of reliable, gridded atmospheric analyses and fields of sea-ice concentration (SIC). We use a stacked and normalized SAT anomaly record (Fig. 2a) based on the six station SAT time series (see Methods) to investigate the broad-scale changes that have affected the northern AP since 1979. To provide an objective measure of the timing of the change in trend we used the sequential Mann–Kendall test (see Methods). This identified the middle of 1998 to early 1999 as the most likely turning point between the warming and cooling periods (indicated by shading on Fig. 2). The trends in the stacked SAT during the warming (0.32 ± 0.20 per decade (dec^{-1}), 1979–1997) and cooling (-0.47 ± 0.25 dec^{-1}, 1999–2014) periods are both statistically significant at $P < 0.05$ (Extended Data Table 1). To confirm that the change in trend is not simply an artefact of the extreme El Niño conditions during 1997–1998, we repeated the analysis for 1979–1996 and 2000–2014. The trends were still significant at $P < 0.05$, although magnitudes were slightly smaller.

While the stacked SAT increased in all seasons during the warming period of 1979–1997 (Extended Data Table 1), the warming was largest during the summer, although the significance of the trend is lower ($P < 0.10$). During this period there was a positive trend in the Southern Annular Mode (SAM)[5], primarily during summer (Extended Data Fig. 1) in response to stratospheric ozone depletion and increasing greenhouse gas concentrations[5,18]. The trend in the SAM led to a greater flow of mild, northwesterly air onto the AP (Extended Data Fig. 2a), with SAT on the northeastern side increasing most because of amplification through the foehn effect[7]. This atmospheric circulation trend contributed to the large decrease in SIC in summer (Extended Data Fig. 3a) and for the year as a whole (Fig. 3a). However, there was no significant trend in annual mean sea-level pressure (SLP) across the AP during the warming period (Fig. 3b). During the summer, tropical climate variability had little influence on the AP SATs[15] and the trend in the SAM had the greatest impact.

Over the cooling period of 1999–2014 there was a significant increase in annual mean SIC around the northern AP and across the northern part of the Weddell Sea (Fig. 3c). This occurred as a result of increasingly cyclonic conditions in the Drake Passage and northwestern Weddell Sea (Fig. 3d), associated with a strengthening mid-latitude jet, which advected cold air towards the AP.

The stacked SAT decreased in all seasons over 1999–2014, but with the greatest cooling during summer, when the trend was moderately significant ($P < 0.10$) (Extended Data Table 1). In this season the trends during the warming and cooling periods are different at a 90% confidence level (see Methods).

During the summer the SAM index remained predominantly positive (Extended Data Fig. 1), and SLP was on average lower over the

[1]British Antarctic Survey, Natural Environment Research Council, High Cross, Madingley Road, Cambridge CB3 0ET, UK.

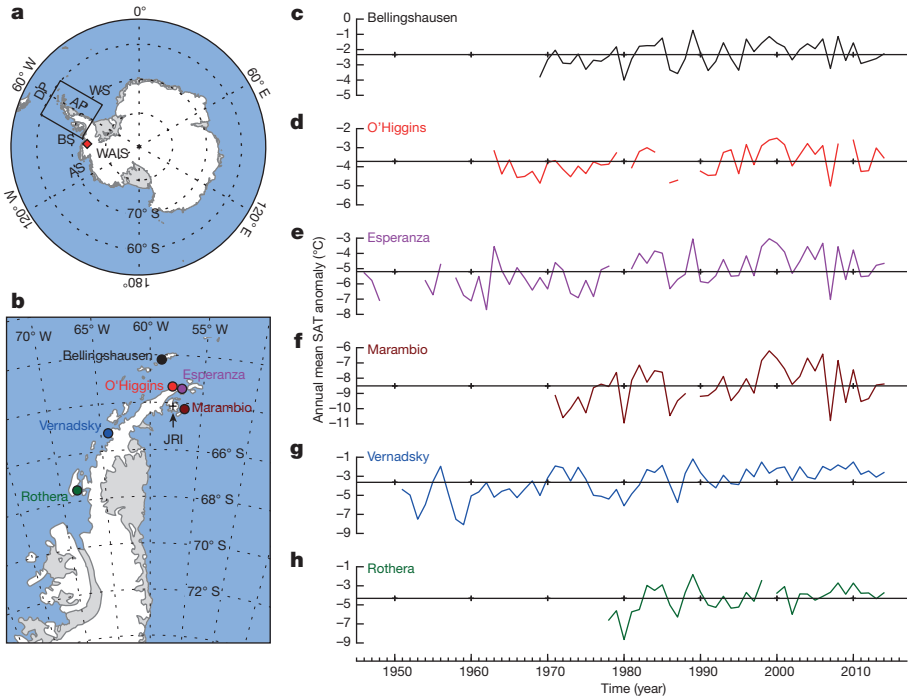

Figure 1 | SAT changes at the six AP stations. **a**, **b**, Map of the Antarctic (**a**) with a blow up of the AP showing the locations of stations referred to in the text (**b**). The locations of the drilling sites for the Ferrigno and James Ross Island ice cores are indicated by a red diamond and an arrowed cross, respectively. **c**–**h**, The time series of annual mean SAT anomalies are shown for Bellingshausen (**c**), O'Higgins (**d**), Esperanza (**e**), Marambio (**f**), Vernadsky (**g**) and Rothera (**h**), with each horizontal line indicating the mean for the whole time series. AS, Amundsen Sea; BS, Bellingshausen Sea; DP, Drake Passage; WAIS, West Antarctic Ice Sheet; WS, Weddell Sea.

Antarctic than during the warming period (Fig. 4a). However, there was no significant trend in the SAM, probably owing to there being little change in the depth of the ozone hole.

The summer cooling resulted from strong east-to-southeasterly near-surface flow towards the AP as SLP decreased (increased) over the South Atlantic (Bellingshausen Sea) (Extended Data Fig. 4a). The greater cyclonic conditions over the South Atlantic occurred in association with a mid-latitude jet that was significantly ($P < 0.05$) stronger than during the warming period (Fig. 4b), and which was located at the northern limit of a cold trough extending from Antarctica. The stronger east-to-southeasterly flow advected sea ice towards the east coast of the AP, giving a positive SIC trend that extended across the whole of the northern Weddell Sea (Extended Data Fig. 5a). This greater ice extent limited the flux of heat from the ocean and amplified the effects of the circulation changes.

During the extended winter, the circulation over the South Pacific is marked by a clearly defined climatological split jet structure, with the subtropical jet (STJ) near 30° S and the polar front jet (PFJ) close to 60° S (ref. 19). The PFJ is sensitive to both zonally symmetric forcing, such as SAM variability, and regional factors, such as the stationary Rossby waves propagating from the tropical Pacific Ocean[15], and the meridional gradient of extratropical SSTs. In general, the STJ (PFJ) is

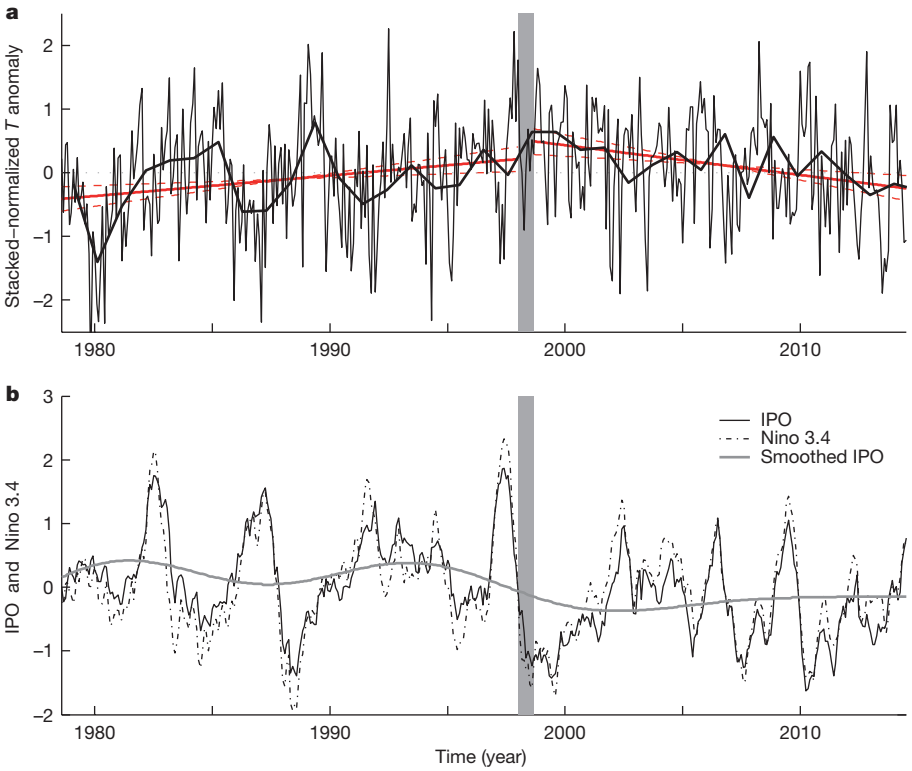

Figure 2 | AP temperature and measures of tropical climate variability since 1979. **a**, The stacked–normalized SAT anomalies for 1979–2014 (thin black line), with the thick black line showing the annual mean values. The solid red lines show the linear trends for the warming and cooling periods, with the 95% confidence limits for the trends indicated by the broken lines. **b**, The monthly mean IPO index (continuous black line) and Niño 3.4 temperature anomaly (broken line), with the grey line showing the IPO index with decadal smoothing. The vertical grey-shaded area on both figures indicates the period of transition from warming to cooling identified by the Mann–Kendall test.

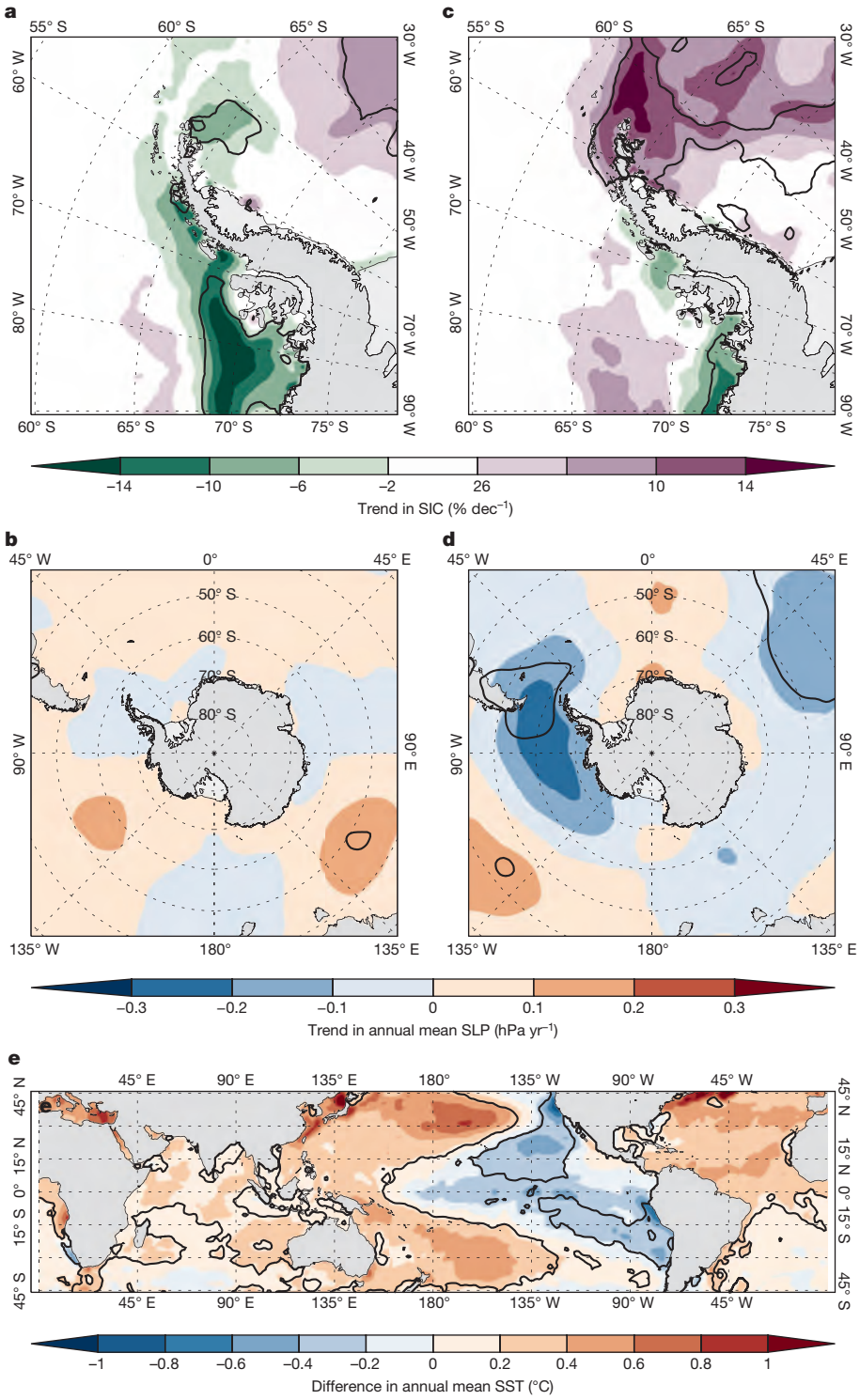

Figure 3 | Trends and differences in atmospheric and oceanic conditions. **a**, The trend in annual mean SIC for 1979–1997. **b**, The trend in annual mean SLP for 1979–1997. **c**, The trend in annual mean SIC for 1999–2014. **d**, The trend in annual mean SLP for 1999–2014. **e**, The difference in annual mean SSTs between 1999–2014 and 1979–1997. Areas where the difference or trend is significant at $P < 0.05$ are indicated by a bold line.

stronger during El Niño/positive Interdecadal Pacific Oscillation (IPO) (La Niña/negative IPO)[20,21]. Nevertheless, their combined effect on the AP regional circulation is complex and may involve nonlinear wave–mean flow feedbacks[22].

The tropical–high-latitude linkages during the extended winter were examined through an analysis of large-scale Rossby wave propagation via the horizontal stationary Eliassen–Palm fluxes[23] at 300 hPa (see Methods). During the 1979–1997 warming period, tropical SSTs were characterized by relatively high SSTs across the eastern tropical Pacific Ocean with relatively more frequent El Niño conditions and a more positive IPO (Fig. 2b), and thus a relatively weak (strong) PFJ (STJ). The generation of quasi-stationary Rossby waves occurred primarily close to 180° E, consistent with higher SSTs in this area, and the wave propagation from the tropics to the South Pacific was limited by a strengthened STJ.

During the 1999–2014 cooling period, a major change in tropical Pacific SSTs occurred with SSTs higher over the Maritime Continent and lower over the eastern Pacific Ocean (Fig. 3e). There was also enhanced transmission of quasi-stationary Rossby waves from the tropics towards the Antarctic, which can be seen in the differences in 300 hPa stream function (Fig. 4f). However, at higher latitudes wave propagation was reduced or prohibited because of enhanced

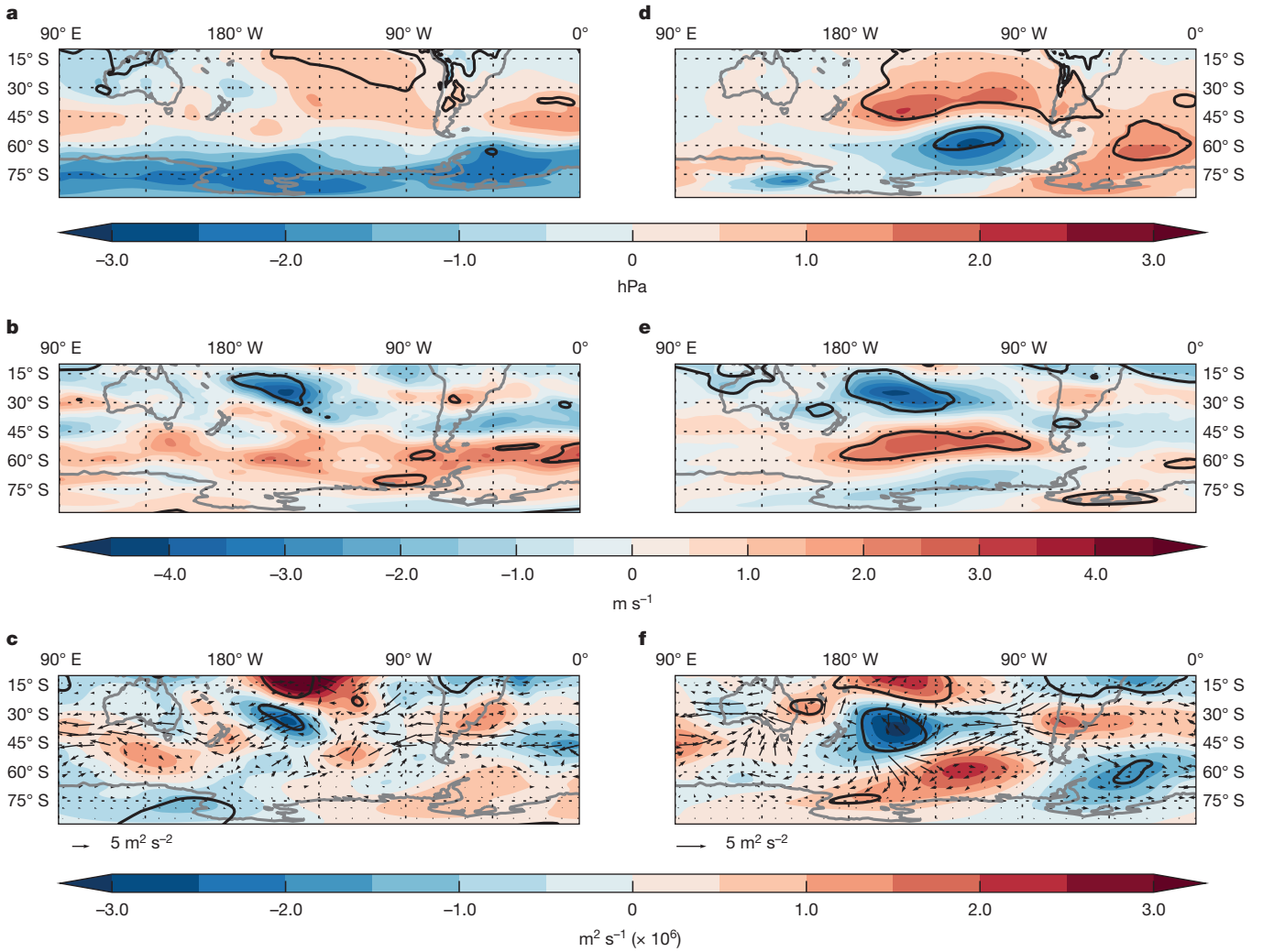

Figure 4 | Differences in atmospheric conditions between the cooling and warming periods (1999–2014 minus 1979–1997). a–f, SLP December–February (DJF) (**a**), 300 hPa zonal wind component DJF (**b**), stream function (colours) and wave propagation (arrows) DJF (**c**), SLP March–September (**d**), 300 hPa zonal wind component March–September (**e**), stream function (colours) and wave propagation (arrows) March–September (**f**). Areas where the differences are significant at $P < 0.05$ are indicated by a bold line.

equatorward wave refraction or reflection from the PFJ region (Fig. 4f). The PFJ was significantly stronger across the South Pacific during the cooling period (Fig. 4e), which is consistent with the higher frequency of La Niña-like conditions and an enhanced meridional temperature gradient between mid- and high latitudes, corresponding to a negative IPO (Fig. 2b). The stronger PFJ resulted in greater surface cyclonic activity to the west of the AP during the cooling period (Fig. 4d), which typically gives higher SATs across the AP[20]. However, critically over 1999–2014 there was a climatological trough in the Drake Passage, giving enhanced easterly flow across the northern Weddell Sea towards the AP. The progressively stronger easterly flow is shown by a decrease of SLP (significant at $P < 0.05$ in March–May (MAM) and June–August (JJA)) in the Drake Passage (Extended Data Fig. 4b–d) and a positive trend in SIC around the northern AP (Extended Data Fig. 5b–d). The cold, east-to-southeasterly circulation negated the warming effect from the tropics usually found in association with La Niña-like conditions, resulting in a cooling trend in SAT during the extended winter period over 1999–2014.

The start of the AP cooling in 1998 coincided with the so-called 'global warming hiatus'. There has been extensive discussion over the factors responsible for this reduction in the rate of increase in mean global SAT[24,25], with the negative phase of the IPO, volcanic and solar activity, and aerosol forcing being cited as possible causes. As discussed earlier, the phase of the IPO can affect the climate of the AP, but the negative phase is usually associated with higher SATs during the extended winter. Since the late 1990s, AP SATs have decreased throughout the year, with local factors playing a greater part than tropical variability, indicating that the absence of AP SAT warming is independent of the global warming hiatus.

The recent change in SAT trend can be set in a longer-term perspective through examination of regional ice core records. An ice core from James Ross Island[26] (Fig. 1), which is close to Marambio station, showed that the region experienced several periods of rapid warming and cooling in the last 1,000 years, and that the warming trend over the last 100 years was 'highly unusual', although not unprecedented. However, the period since the late 1970s includes the ozone hole, which is unique in the record. The Ferrigno ice core from the coast of West Antarctica (Fig. 1) shows a warming from the 1950s to the early twenty-first century that agrees well with the warming observed at Vernadsky[27]. In the longer term, this record revealed marked decadal variability and, importantly, resolved a 50-year period in the eighteenth century when SATs increased at a faster rate than observed at Vernadsky over the second half of the twentieth century. Such long-term variability is also expected from analysis of station SAT records, which exhibit statistical long-term persistence[28]. Therefore all these studies suggest that the rapid warming on the AP since the 1950s and subsequent cooling since the late-1990s are both within the bounds of the large natural decadal-scale climate variability of the region. This result is also consistent with

the very high level of decadal-scale natural internal variability of the regional atmospheric circulation seen in long control runs of climate models[29]. Climate model projections forced with medium emission scenarios indicate the emergence of a large anthropogenic regional warming signal, comparable in magnitude to the late twentieth century Peninsula warming, during the latter part of the current century[30].

Online Content Methods, along with any additional Extended Data display items and Source Data, are available in the online version of the paper; references unique to these sections appear only in the online paper.

Received 5 February; accepted 6 June 2016.

1. Turner, J. *et al.* Antarctic climate change during the last 50 years. *Int. J. Climatol.* **25,** 279–294 (2005).
2. Cook, A. J., Fox, A. J., Vaughan, D. G. & Ferrigno, J. G. Retreating glacier fronts on the Antarctic Peninsula over the past half-century. *Science* **308,** 541–544 (2005).
3. Vaughan, D. G. Implications of the break-up of Wordie Ice Shelf, Antarctica for sea level. *Antarct. Sci.* **5,** 403–408 (1993).
4. Convey, P. in *Antarctic Peninsula Climate Variability: Historical and Palaeoenvironmental Perspectives* (eds Domack, E. *et al.)* 145–158 (American Geophysical Union, 2003).
5. Thompson, D. W. J. & Solomon, S. Interpretation of recent Southern Hemisphere climate change. *Science* **296,** 895–899 (2002).
6. Turner, J., Maksym, T., Phillips, T., Marshall, G. J. & Meredith, M. P. Impact of changes in sea ice advance on the large winter warming on the western Antarctic Peninsula. *Int. J. Climatol.* **33,** 852–861 (2013).
7. Marshall, G. J., Orr, A., van Lipzig, N. P. M. & King, J. C. The impact of a changing Southern Hemisphere Annular Mode on Antarctic Peninsula summer temperatures. *J. Clim.* **19,** 5388–5404 (2006).
8. Ding, Q., Steig, E. J., Battisti, D. S. & Kuttel, M. Winter warming in West Antarctica caused by central tropical Pacific warming. *Nature Geosci.* **4,** 398–403 (2011).
9. Clem, K. R. & Fogt, R. L. Varying roles of ENSO and SAM on the Antarctic Peninsula climate in austral spring. *J. Geophys. Res. Atmos.* **118,** 11481–11492 (2013).
10. Brohan, P., Kennedy, J. J., Harris, I., Tett, S. F. B. & Jones, P. D. Uncertainty estimates in regional and global observed temperature changes: a new data set from 1850. *J. Geophys. Res. Atmos.* **111,** D12106 (2006).
11. Screen, J. A. & Simmonds, I. The central role of diminishing sea ice in recent Arctic temperature amplification. *Nature* **464,** 1334–1337 (2010).
12. Vaughan, D. G. *et al.* Recent rapid regional climate warming on the Antarctic Peninsula. *Clim. Change* **60,** 243–274 (2003).
13. Bromwich, D. H. *et al.* Central West Antarctica among the most rapidly warming regions on Earth. *Nature Geosci.* **6,** 139–145 (2013).
14. Connolley, W. M. Variability in annual mean circulation in southern high latitudes. *Clim. Dyn.* **13,** 745–756 (1997).
15. Trenberth, K. E., Fasullo, J. T., Branstator, G. & Phillips, A. S. Seasonal aspects of the recent pause in surface warming. *Nature Clim. Chang.* **4,** 911–916 (2014).
16. Li, X. C., Holland, D. M., Gerber, E. P. & Yoo, C. Impacts of the north and tropical Atlantic Ocean on the Antarctic Peninsula and sea ice. *Nature* **505,** 538–542 (2014).
17. Carrasco, J. F. Decadal changes in the near-surface air temperature in the western side of the Antarctic Peninsula. *Atmos. Clim. Sci* **3,** 275–281 (2013).
18. Gillett, N. P. *et al.* Attribution of polar warming to human influence. *Nature Geosci.* **1,** 750–754 (2009).
19. Bals-Elsholz, T. M. *et al.* The wintertime Southern Hemisphere split jet: structure, variability, and evolution. *J. Clim.* **14,** 4191–4215 (2001).
20. Turner, J. The El Niño-Southern Oscillation and Antarctica. *Int. J. Climatol.* **24,** 1–31 (2004).
21. Chen, B., Smith, S. R. & Bromwich, D. H. Evolution of the tropospheric split jet over the South Pacific Ocean during the 1986–89 ENSO cycle. *Mon. Weath. Rev.* **124,** 1711–1731 (1996).
22. Lorenz, D. J. & Hartmann, D. L. Eddy-zonal flow feedback in the Northern Hemisphere winter. *J. Clim.* **16,** 1212–1227 (2003).
23. Plumb, R. A. On the 3-dimensional propagation of stationary waves. *J. Atmos. Sci.* **42,** 217–229 (1985).
24. Fyfe, J. C. *et al.* Making sense of the early-2000s warming slowdown. *Nature Clim. Chang.* **6,** 224–228 (2016).
25. Trenberth, K. E. Has there been a hiatus ? *Science* **349,** 691–692 (2015).
26. Mulvaney, R. *et al.* Recent Antarctic Peninsula warming relative to Holocene climate and ice-shelf history. *Nature* **489,** 141–144 (2012).
27. Thomas, E. R., Bracegirdle, T. J., Turner, J. & Wolff, E. W. A 308 year record of climate variability in West Antarctica. *Geophys. Res. Lett.* **40,** 5492–5496 (2013).
28. Ludescher, J., Bunde, A., Franzke, C. L. E. & Schellnhuber, H. J. Long-term persistence enhances uncertainty about anthropogenic warming of Antarctica. *Clim. Dyn.* **46,** 263–271 (2016).
29. Turner, J., Hosking, J. S., Marshall, G. J., Phillips, T. & Bracegirdle, T. J. Antarctic sea ice increase consistent with intrinsic variability of the Amundsen Sea Low. *Clim. Dyn.* **46,** 2391–2402 (2016).
30. Bracegirdle, T. J., Connolley, W. M. & Turner, J. Antarctic climate change over the Twenty First Century. *J. Geophys. Res.* **113,** D03103 (2008).

Supplementary Information is available in the online version of the paper.

Acknowledgements This work was financially supported by the UK Natural Environment Research Council under grant NE/K00445X/1. It forms part of the Polar Science for Planet Earth programme of the British Antarctic Survey. We are grateful to D. G. Vaughan for valuable discussions during this study. We are grateful to ECMWF for the provision of reanalysis fields and to the US National Snow and Ice Data Center for the sea-ice data. The data used in this study are available from the authors upon request.

Author Contributions J.T. conceived the study and led the writing of the manuscript. J.T., H.L., T.P., J.S.H., G.J.M., T.J.B. and J.C.K. analysed the results. P.D. investigated the role of tropical forcing. T.P. managed the data and prepared some of the figures. H.L. carried out the statistical analysis. R.M. compared the recent trends with palaeoclimate data. I.W. computed the stationary eddy fluxes.

Author Information Reprints and permissions information is available at www.nature.com/reprints. The authors declare no competing financial interests. Readers are welcome to comment on the online version of the paper. Correspondence and requests for materials should be addressed to J.T. (jtu@bas.ac.uk).

Reviewer Information *Nature* thanks W. Hobbs and E. Steig for their contribution to the peer review of this work.

METHODS

Data. The monthly mean SAT data for the stations were obtained primarily from the Scientific Committee on Antarctic Research (SCAR) Reference Antarctic Data for Environmental Research (READER) data base[31]. These values are derived as the mean of the synoptic (6-hourly) observations. A monthly value was produced only if 90% of the 6-hourly data were available. To maximize the number of these data, if a value was missing, but adjacent 3-hourly values were available, then an estimate of the 6-hourly value was made by linearly interpolating between these two adjacent values; for example, if a value at 06Z was missing but values existed at 03Z and 09Z then the mean of those values would be used to estimate a value for 06Z. Any resultant bias will be random and should have a negligible effect on the monthly mean. Similar to READER, if there were insufficient synoptic observations to derive a monthly mean, a value was taken from the monthly CLIMAT message if available.

To account for differences in temperature variability between the six stations, we have generated a monthly mean stacked SAT anomaly record. These values are the mean of the available normalized temperature anomalies, of which at least five are available from 1979 onwards. Anomalies are calculated relative to the 1981–2010 period. Our use of the stacked temperature anomalies is justified by the fact that SATs at all six stations have a similar relationship to mean SLP (Extended Data Fig. 6) and therefore the broad-scale atmospheric circulation, despite there being differences in local effects. Indeed, Ding and Steig[32] also demonstrated that trends computed from a stacked AP SAT record showed good, broad-scale agreement with trends determined from satellite and reanalysis data.

To investigate atmospheric circulation variability for 1979–2014, we use the fields from the European Centre for Medium-range Weather Forecasting (ECMWF) Interim reanalysis (ERA-Interim), which have a grid spacing of $0.7° \times 0.7°$ and are considered to be the best reanalysis for depicting recent Antarctic climate[33]. Fields of mean SIC, computed using the Bootstrap version 2 algorithm[34] were obtained on a 25-km-resolution grid from the US National Snow and Ice Data Center (http://www.nsidc.org).

Statistical methods. A non-parametric statistical technique called the sequential Mann–Kendall test[35–37] was employed to detect the period when a significant change of trend occurred in the monthly mean stacked temperature anomalies. Note that the sequential Mann–Kendall test has been widely used to detect approximate potential trend turning points in time series[36–38].

The null hypothesis we tested was that there is no turning point in the trend of the monthly temperature anomaly time series under investigation. To prove or to disprove the null hypothesis, our calculation follows the procedure given by Gerstengarbe and Werner[36]. Let a temperature time series $X=\{X_1,\ldots, X_n\}$ be separated into $n-1$ subseries (that is, the first subseries includes the sample values $X_1, X_2,\ldots$, the second include the values $X_2, X_3,\ldots$, and so on). The $n-1$ Mann–Kendall test statistic variables[35] determined by these subseries are given as:

$$W_t = \sum_{i=1}^{t} R_i$$

where R_i is the rank of the *t-th* sub-series $\{X_1, X_2,\ldots, X_{t+1}\}$, that is, the number of the elements $X_i\{i>j\}$ such that $X_i > X_j$ with $i=2,\ldots, t$ and $j=1,\ldots, i-1$. Consequently, for each of the $n-1$ subseries, the corresponding progressive row $U(t)$ is defined as

$$U(t) = \frac{W_t - E(W_t)}{\sqrt{\mathrm{Var}(W_t)}}$$

where $E(W_t)$ is the expected value of the respective subseries with

$$E(W_t) = \frac{l_t(l_t-1)}{4}$$

and $\mathrm{Var}(W_t)$ is the respective variance given by

$$\mathrm{Var}(W_t) = \frac{l_t(l_t-1)(2l_t-5)}{72}$$

which assumes that, for $l_t \to \infty$ (l_t = the length of the subseries), W_t is approximately Gaussian and the normalized $U(t)$ is assumed to be a standard Gaussian distribution. Similarly, for a given t, the corresponding rank series $V(t)$, the so-called retrograde row can be calculated using the reversed time series $\{X_{t+1}, X_{t-2},\ldots, X_1\}$.

Once the progressive and retrograde rank series $U(t)$ and $V(t)$ are calculated for all $t=1,\ldots, n-1$, the temporal locations where $U(t)$ and $V(t)$ cross each other are determined and considered as potential trend turning points. When either the progressive $U(t)$ or retrograde $V(t)$ row exceeds certain confidence limits (for example, the absolute values of $U(t)$ and $V(t)$ become greater than 2 in our case) before and after the crossing point, the null hypothesis that the sampled time series has no change points is rejected.

The statistical significance of the linear trends during the warming and cooling periods is estimated using the non-parametric Mann–Kendall Tau and Sens slope test[36,38], where the *P* values are calculated as two-sided. To test the significance of the trend differences between two periods, we compute the confidence intervals at 90% and 95% levels for individual trends and examine whether or not they overlap[39].

As the sequential Mann–Kendall test can only detect the approximate time when a change of the trend may occur, we find that it is often the case that multiple changes can be detected over a couple of years. Namely, the trend change may actually take a couple of years to occur in the real world.

Correlations, linear trends and composite differences from gridded data sets were computed using monthly anomalies based on a standard least-squares method, with the methodology used to calculate the significance levels based upon Santer *et al.*[39]. An effective sample size was calculated based on the lag 1 autocorrelation coefficient of the regression residuals. This effective sample size was used for the computation of the standard error and in indexing the critical values of Student's *t* distribution. On figures showing the differences of means between the warming and cooling periods, significance levels were calculated using *t*-tests performed without the assumption of equal variances between the periods being compared. For the computation of the correlations, the time series of SST and atmospheric fields were all detrended.

Determination of the stationary wave fluxes. The formulation of Plumb[23] was used to estimate the difference in stationary wave activity between the warming and cooling periods in the upper troposphere (for example, 300 hPa). The fluxes give an indication of the direction of wave propagation and take the form:

$$\mathbf{F} = \frac{p\cos\varphi}{2}\left(v'^2 - \frac{\Phi'}{af\cos\varphi}\frac{\partial v'}{\partial\lambda},\ -v'u' + \frac{\Phi'}{af\cos\varphi}\frac{\partial u'}{\partial\lambda}\right)$$

where λ, φ are the zonal and meridional coordinates, u, v are the zonal and meridional velocity components, p represents normalized pressure, which is pressure divided by a standard reference pressure p_s, here p_s is taken as 1,000 hPa, a is the Earth's radius, $f=2\Omega\sin\varphi$ is the Coriolis parameter with Ω the Earth's rotation rate and Φ the geopotential. Primes represent deviations from the zonal-mean. Note that **F** has been written in terms of the geopotential Φ by using the geostrophic wind relations $u = -\frac{\psi_\varphi}{a}$, $v = \frac{\psi_\lambda}{a\cos\varphi}$, where ψ is the geostrophic stream function. This is to reduce the possible amplification of noise due to successive derivatives and to facilitate the physical understanding of each components. All differentiation is performed using centred differences. Also, **F** is calculated on a monthly basis to isolate the stationary perturbations and then a time-average is taken over the selected period for each year.

31. Turner, J. *et al.* The SCAR READER project: towards a high-quality database of mean Antarctic meteorological observations. *J. Clim.* **17,** 2890–2898 (2004).
32. Ding, Q. H. & Steig, E. J. Temperature change on the Antarctic Peninsula linked to the tropical Pacific. *J. Clim.* **26,** 7570–7585 (2013).
33. Bracegirdle, T. J. & Marshall, G. J. The reliability of Antarctic tropospheric pressure and temperature in the latest global reanalyses. *J. Clim.* **25,** 7138–7146 (2012).
34. Comiso, J. C. Variability and trends in Antarctic surface temperatures from *in situ* and satellite infrared measurements. *J. Clim.* **13,** 1674–1696 (2000).
35. Mann, H. B. Non parametric test against trend. *Econometric* **13,** 245–259 (1945).
36. Gerstengarbe, F. W. & Werner, P. C. Estimation of the beginning and end of recurrent events within a climate regime. *Clim. Res.* **11,** 97–107 (1999).
37. Li, Y., Lu, H., Jarvis, M. J., Clilverd, M. A. & Bates, B. Nonlinear and nonstationary influences of geomagnetic activity on the winter North Atlantic Oscillation. *J. Geophys. Res. Atmos.* **116,** D16109 (2011).
38. Burkey, J. A non-parametric monotonic trend test computing Mann-Kendall Tau, Tau-b, and Sens Slope written in MathWorks MATLAB (King County, Department of Natural Resources and Parks, Science and Technical Services section, 2006).
39. Santer, B. D. *et al.* Statistical significance of trends and trend differences in layer-average atmospheric temperature time series. *J. Geophys. Res.* **105,** 7337–7356 (2000).
40. Marshall, G. J. Trends in the Southern Annular Mode from observations and reanalyses. *J. Clim.* **16,** 4134–4143 (2003).

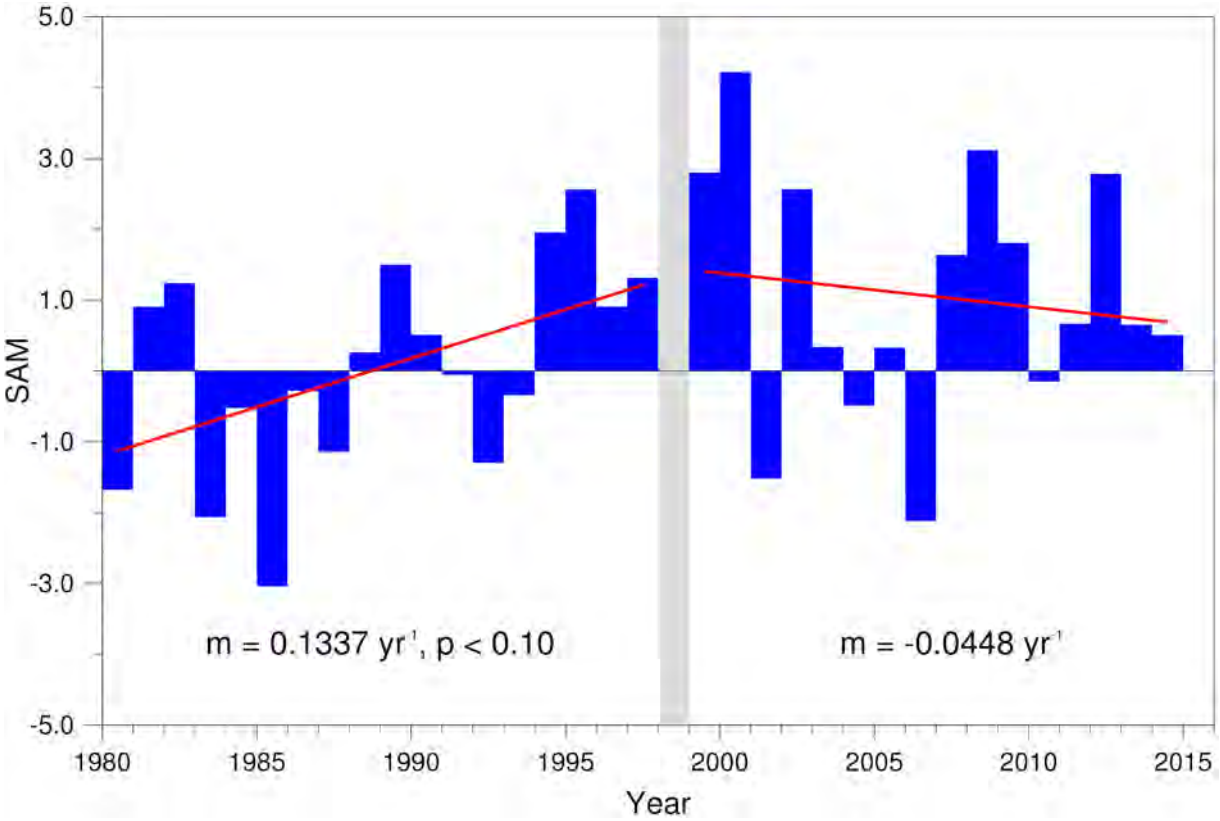

Extended Data Figure 1 | The Southern Annular Mode. The austral summer (December–February) SAM index[40] for December 1979–February 2014. The linear trends for 1980–1997 and 1999–2014 are shown in red. The data were obtained from https://legacy.bas.ac.uk/met/gjma/sam.html.

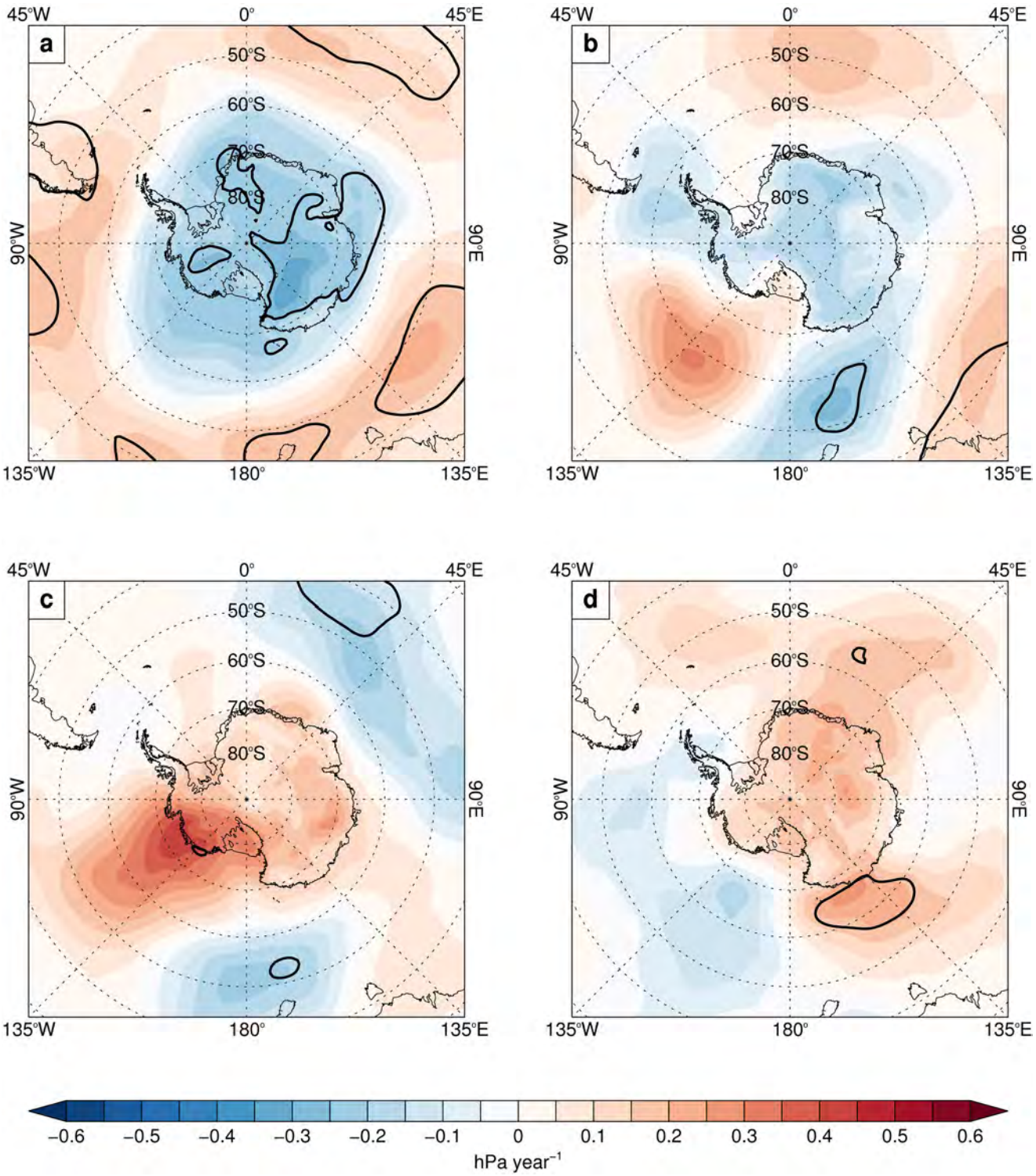

Extended Data Figure 2 | Seasonal SLP trends during the warming period. a–d, DJF December 1979–February 1998 (**a**), MAM 1979–1997 (**b**), JJA 1979–1997 (**c**) and September–November (SON) 1979–1997 (**d**). Areas where the trends are significant at $P < 0.05$ are indicated by a bold line.

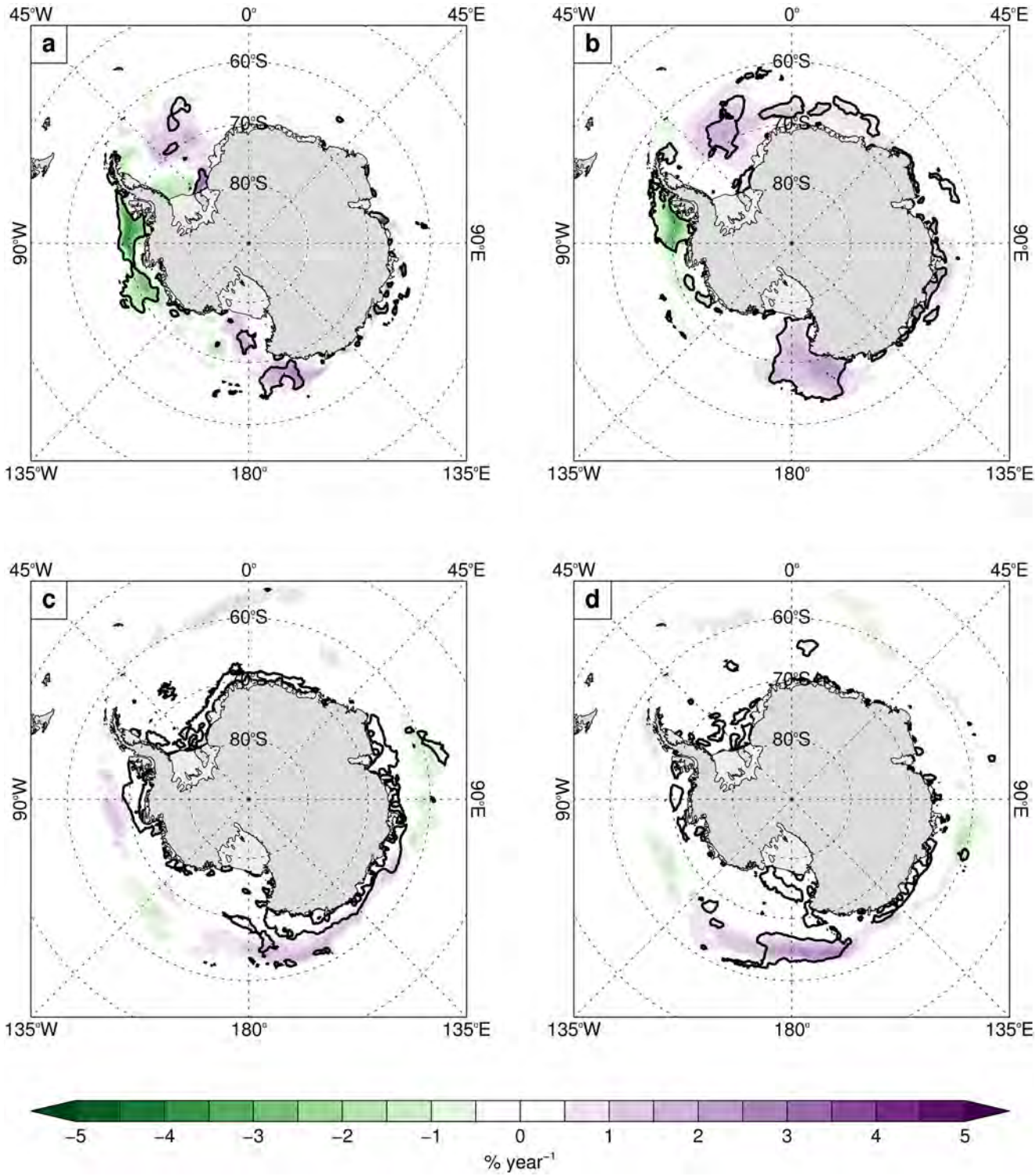

Extended Data Figure 3 | Seasonal trends in sea-ice concentration during the warming period. a–d, DJF December 1979–February 1998 (**a**), MAM 1979–1997 (**b**), JJA 1979– 1997 (**c**) and SON 1979–1997 (**d**). Areas where the trends are significant at $P < 0.05$ are indicated by a bold line.

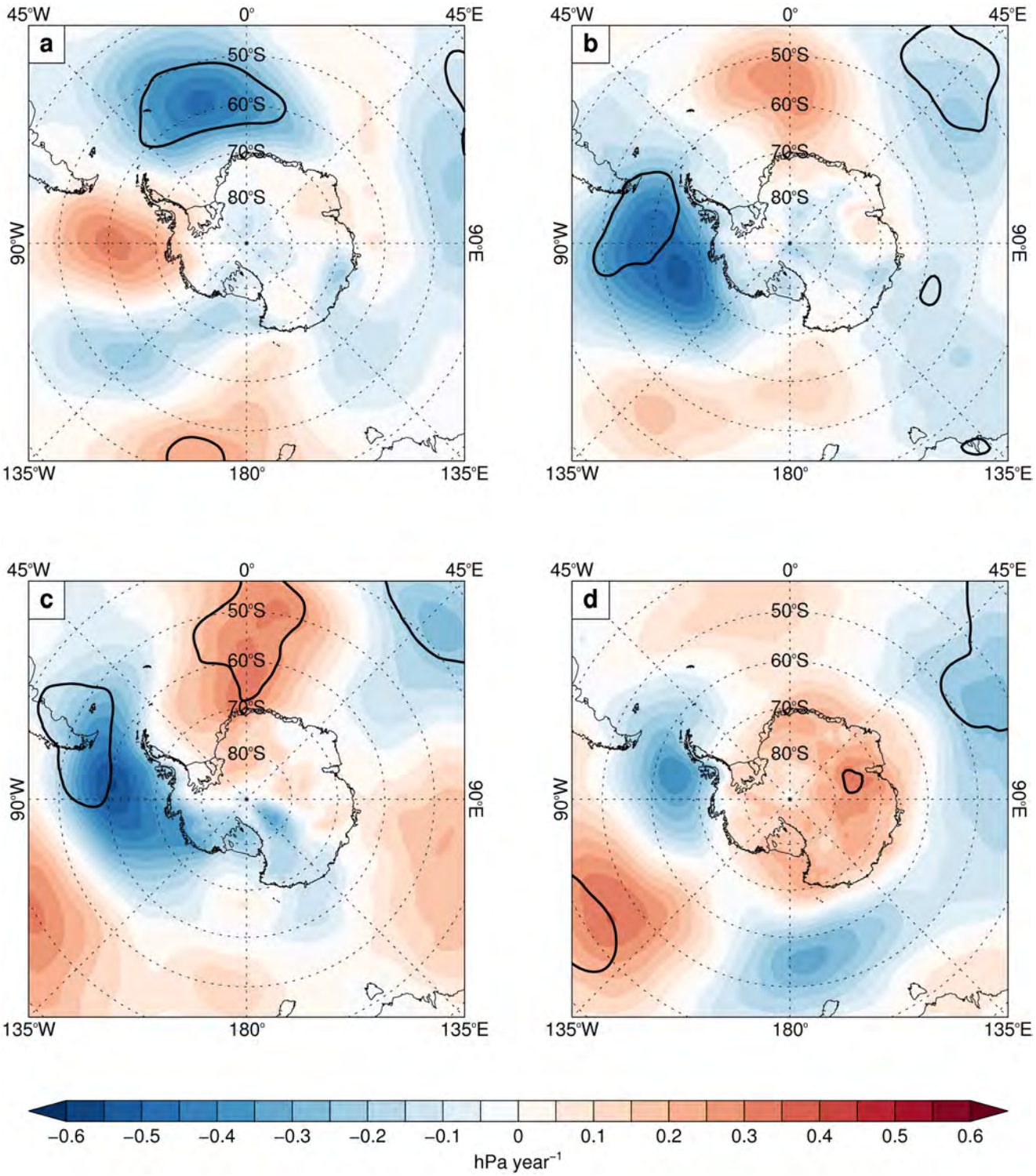

Extended Data Figure 4 | Seasonal SLP trends during the cooling period. a–d, DJF December 1999–February 2014 (**a**), MAM 1999–2014 (**b**), JJA 1999–2014 (**c**) and SON 1999–2014 (**d**). Areas where the trends are significant at $P < 0.05$ are indicated by a bold line.

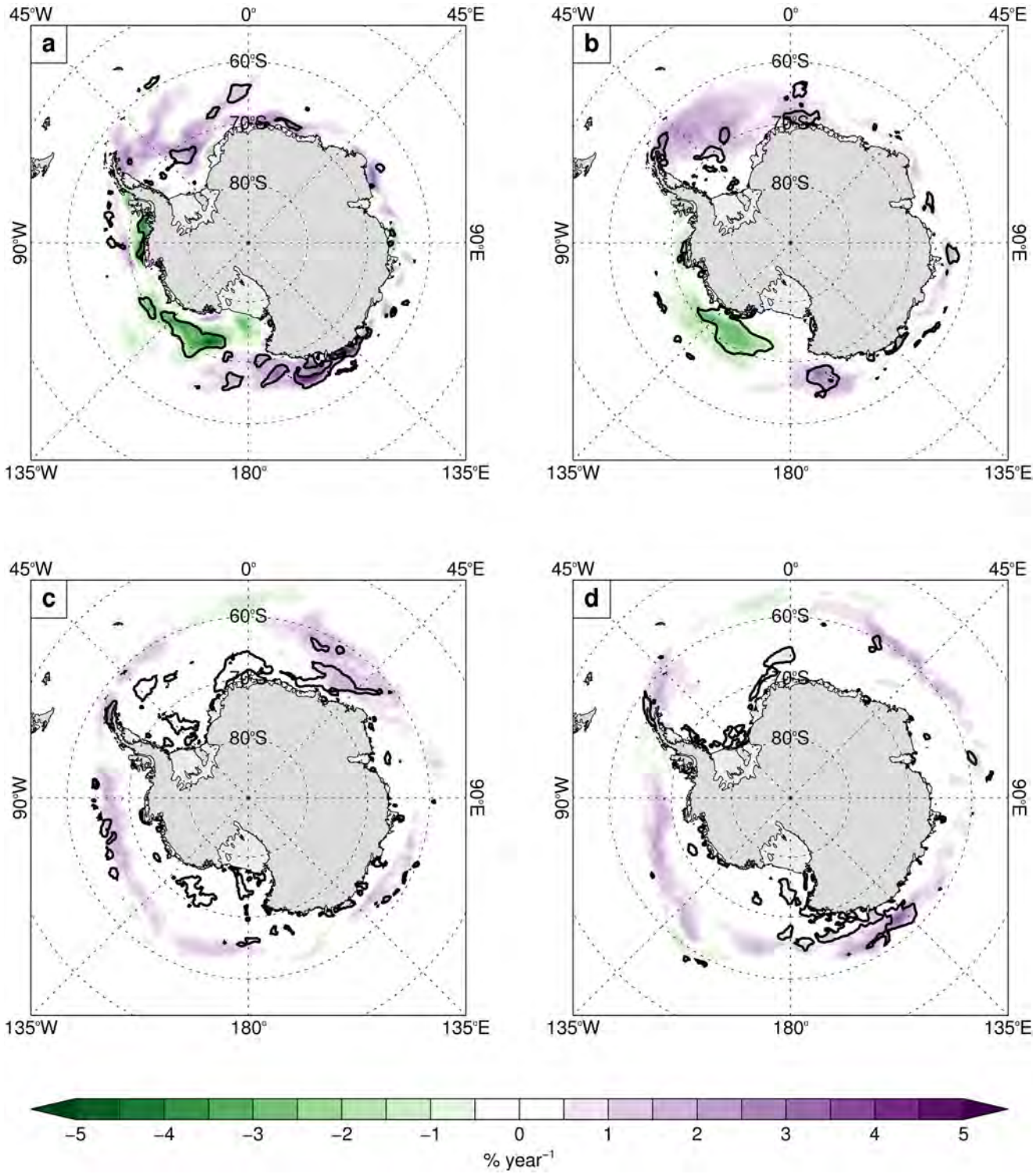

Extended Data Figure 5 | Seasonal trends in sea-ice concentration during the cooling period. a–d, DJF December 1999–February 2014 (**a**), MAM 1999–2014 (**b**), JJA 1999–2014 (**c**) and SON 1999–2014 (**d**). Areas where the trends are significant at $P < 0.05$ are indicated by a bold line.

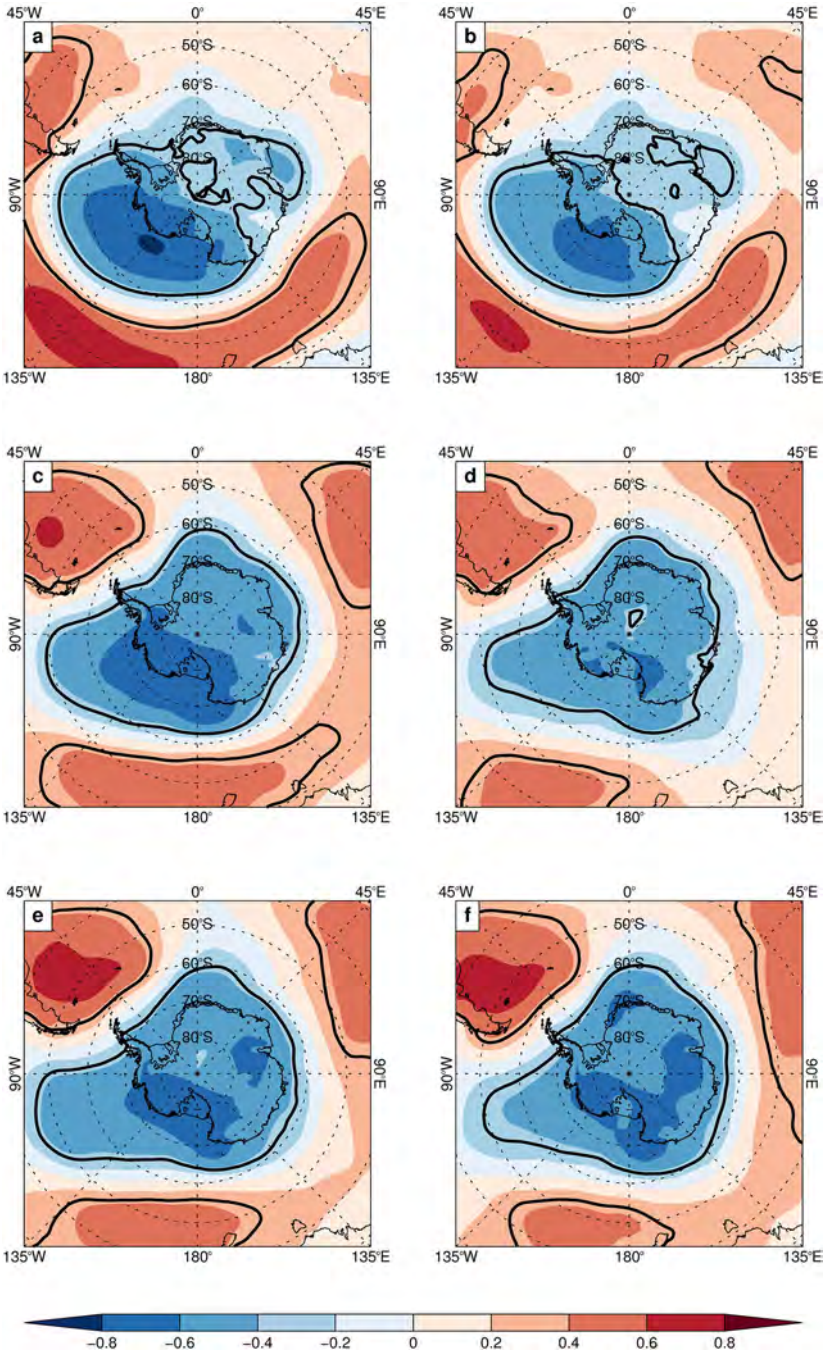

Extended Data Figure 6 | The correlation of annual mean SAT from the stations with annual mean SLP for 1979–2014. a–f, Areas where the correlation is significant at $P < 0.05$ are indicated by a bold line. Rothera (**a**), Vernadsky (**b**), Bellingshausen (**c**), O'Higgins (**d**), Esperanza (**e**) and Marambio (**f**).

Extended Data Table 1 | Annual and seasonal trends of the stacked, normalized temperature record

	Annual	DJF	MAM	JJA	SON
1979 – 1997	0.32**	0.51*	0.18	0.04	0.33
1999 - 2014	-0.47**	-0.72*	-0.39	-0.09	-0.36

Trends are given for the warming (1979–1997) and cooling (1999–2014) periods and are per decade. Significance of the trends is indicated as $^{**}P < 0.05$ and $^{*}P < 0.10$. Note, the DJF trends are for the summer seasons over December 1979–February 1998 and December 1999–February 2014.